On the saltation of fresh snow in a wind tunnel: Profile characterization and single particle statistics

M. Guala,[1,2] C. Manes,[1] A. Clifton,[1,3] and M. Lehning[1]

[1]   We present experimental results on the snow drift in a turbulent boundary layer over a flat fresh snow-covered surface. Vertical profiles of mass flux and of the distribution of particle diameters were obtained by means of a pair of Snow Particle Counters parallel with measurements of the stream-wise velocity profile. The aim of the paper is to discuss current parameterizations of the vertical mass flux profile for fresh snow and to investigate the range of timescales involved in a developing saltation layer occurring in a turbulent boundary layer. The novelty of the work consists of using an intact fresh snow cover as an erodible surface able to provide realistic snow crystals as drifting particles. Results show that (1) the parameters scaling the vertical mass flux profiles of fresh snow can significantly differ from those given in the literature for ice or compacted snow particles; (2) though drifting snow covers an extremely wide range of temporal scales, the mean time interval between saltating particles $\langle \Delta t \rangle$ is the key timescale of the saltation process; (3) $\langle \Delta t \rangle$ allows for the optimal reconstruction of the mass flux as a continuous signal and for neglecting the effects related to the heterogeneous distribution of particle size on the mass flux. Implications on the modeling of snow drift and on the processing of field observations are discussed.

1. Introduction

[2]   The physics of drifting snow combines complex phenomena spanning from two phase turbulent boundary layers [see, e.g., *Araoka and Maeno*, 1981; *Nishimura and Hunt*, 2000; *Nishimura and Nemoto*, 2005] erosion and deposition processes at the surface (*Anschutz et al.* [2006], *Li and Sturm* [2002], and *Massom et al.* [1998] among others), saltation and collisions of fragile particles [see *Pomeroy and Gray*, 1990; *Nemoto and Nishimura*, 2001; *Doorschot and Lehning*, 2002; *Clifton and Lehning*, 2008, and reference therein], snow metamorphism [e.g., *Lehning et al.*, 2002] and mechanisms related to dispersed particle sizes [see *Maeno et al.*, 1995; *Sugiura et al.*, 1998]. The complexity is further increased by a nontrivial interplay between different length and timescales phenomena. Moreover, snow drift usually occurs in nature in complex environments, i.e., in strongly three dimensional topographies, with unsteady boundary conditions (varying wind velocity and direction, air temperature, pressure, humidity and thus varying snow properties) and very often during snow fall [see, e.g., *Schmidt*, 1982; *Lehning et al.*, 2007]. In the context of investigating fundamental issues related to the physics of drifting snow and the mutual interaction between wind and particle entrainment, it is then desirable to simplify the problem and perform experiments in a controlled environment, i.e., under monitored and, to some extent, steady boundary conditions. This can be achieved in the Swiss Federal Institute for Snow and Avalanche Research cold wind tunnel [*Clifton et al.*, 2006]. This facility is designed to work at low temperature conditions, to collect and store fresh snow during snow precipitation and to place it inside the wind tunnel without altering the three dimensional structure of the naturally deposited snow cover. It is therefore possible to reproduce drifting conditions in the saltation regime for a wide range of natural snow types, air velocities and temperatures. *Clifton et al.* [2006] determined the shear stress threshold of snow motion through a series of wind tunnel experiments at increasing velocity. *Clifton and Lehning* [2008] were devoted to the modeling of snow drift and characterized by a physical and statistical description of the Lagrangian motion of the saltating particles. However, accurate experimental observations are still needed in order to improve the physical description of the motion of the single particles and better justify the underlying assumptions in the models. The focus of the present paper is thus to present a state of the art accurate description of the snow drift occurring in a wind tunnel over fresh snow. The main goals are to provide (1) a benchmark of experimental observations, emphasizing the complexity and the variety of length and especially timescales of snow drift in saltation regiment and (2) the statistical tools to assess the optimal

[1]Swiss Federal Institute for Snow and Avalanche Research, Davos, Switzerland.
[2]California Institute of Technology, Pasadena, California, USA.
[3]University of Northern British Columbia, Prince George, British Columbia, Canada.

temporal resolution of the mass flux as a function of the mean time interval between saltating particle and of their size distribution. Particular attention is devoted to the estimation of the vertical mass flux density profile, its parameterizations and ultimately its effect on the saltation length scale. The novelty of the work lies in the fact that all this analysis is performed for real snow for which detailed experimental laboratory data are missing in literature. High- (40 kHz) and low-frequency (1 Hz) measurements of mass flux and particle diameters were obtained at different vertical locations by means of two synchronized Niigata Company Snow Particle Counters (SPC) together with the mean flow velocity and mean temperature. SPC technology is robust, well established and it allows the comparison between wind tunnel [*Clifton et al.*, 2006] and field data (see, e.g., measurements in the alpine regions [*Doorschot and Lehning*, 2002; *Doorschot et al.*, 2004], or in Antartica [*Nishimura and Nemoto*, 2005]. Furthermore SPC provides an estimate of the particle size [see, e.g., *Sugiura et al.*, 1998] and thus allows to focus on the different behavior of large and small particles that might ultimately have implications on the collision and splash mechanisms as well as on surface armoring, particles trapping, and sorting effects. We expect that snow drift occurs over a wide range of timescales ranging from the time interval between saltating particles to the timescales of the morphodynamic evolution of large-scale surface features as dunes or sediment waves. It thus includes all the scales displayed by a turbulent boundary layer [see, e.g., *Guala et al.*, 2006; *Balakumar and Adrian*, 2007]. The analysis presented here aims at selecting, among all these timescales, the one representative of the saltation process, and to relate it to an optimal definition of the mass flux. We further extend this study to the characteristic behavior of fine and coarse particles. We indeed estimate the averaging timescale at which (1) the observed differences between particle size fluxes become negligible and thus (2) the assumption of a monodispersed distribution of particle sizes allows for a correct estimate of the mass flux. The implications on the assumptions of monodispersed size particles and continuous mass flux function, for snow drift modeling over large scales are discussed.

[3]   After this introduction, the experimental apparatus will be briefly described and the procedure to obtain and validate the high- frequency measurements from the SPC will be provided in the next section. The description of the results is then divided into a low-frequency subsection (profiles of the mean mass flux and diameter distribution) and a high-frequency subsection (interparticle time interval, definition of a high-frequency mass flux and of the contribution by the fine and the coarse snow particle fractions). The last section is devoted to discussions and conclusions.

2.   Experimental Apparatus

2.1.   Wind Tunnel

[4]   All the experiments were carried out at the Swiss Federal Institute for Snow and Avalanche Research wind tunnel located in Davos, Switzerland at 1670 m a.s.l. [see *Clifton et al.*, 2006]. The wind tunnel operates in suction mode and it is 14m long with a 1×1 m cross section. The air is drawn from the outside and goes through an inlet

composed of a honeycomb net and 4:1 contraction. Downstream of the contraction, the air flows through vertical spires and over 4 m of regular roughness elements. These are followed by 4 m of a carpet surface before the flow hits the snow surface. This flow conditioning was designed to create a turbulent boundary layer with a logarithmic region of 0.25 m depth and hence to contain the saltation layer developing over the snow. This, beside reproducing natural conditions occurring in the atmosphere also prevents/limits the snow transport in the suspension regime. The necessary steps of the full experimental procedure can be summarized in the following: (1) at least 10 cm of fresh snow is collected outside the wind tunnel in flat, purpose built, trays where, providing the absence of wind, the snow surface remains substantially flat with spatially homogeneous roughness characteristics; (2) the trays are carefully moved inside the wind tunnel so that the intact, snow surface layer becomes the lower boundary conditions for the flow; (3) the height of the snow cover is adjusted to the fixed floor of the wind tunnel upstream section; (4) a turbulent boundary layer is generated within the wind tunnel and velocities tuned to the point at which there is substantial snow transport. Mean velocity and mass flux profiles are then measured by means of digital anemometers ("MiniAir") and SPC ("Niigata Company") respectively. Provided the ambient temperature is low enough and in equilibrium with the outside air temperature, snow metamorphism processes occurring in the test section of the wind tunnel are minimized and comparable with those occurring outside. As a result of the whole experimental procedure the snow drift observed in the wind tunnel is qualitatively and quantitatively representative of the snow drift observed in nature during or immediately after a calm snowfall. The boundary and environmental conditions, (necessary for the calculation of the air properties such as density) are monitored through a Meteo station located on the roof of the building. This is equipped with temperature humidity and pressure sensors and a snow height sensor located in the proximity of the fresh snow collection and storage facility. Such data are accessible on remote and allow not only an optimal planning of the experiment but also a continuous monitoring of the environmental conditions at the measuring site during snow fall before and during the experiments. Temperature and humidity sensors are also located in the building at the wind tunnel inlet. Before each experiment, the room is ventilated until the inside and outside temperature and humidity sensors display the same values. In the following text we focus on the latest improvements in the measuring and data acquisition setup. In particular we explain the calibration and acquisition of the high-frequency signal from the SPC.

2.2.   Vertical Profiles: Spatial and Temporal Limitations

[5]   Measurements of snow particle mass flux and diameter were performed by means of two synchronized (Niigata Company) Snow Particle Counters [see, e.g., *Sugiura et al.*, 1998; *Nishimura and Nemoto*, 2005]. One SPC was kept at a fixed location to monitor the large timescale variations of the mass flux, while the second SPC was allowed to move in the wall normal direction, from a few centimeters above surface up to the top of the saltation layer. The motivation
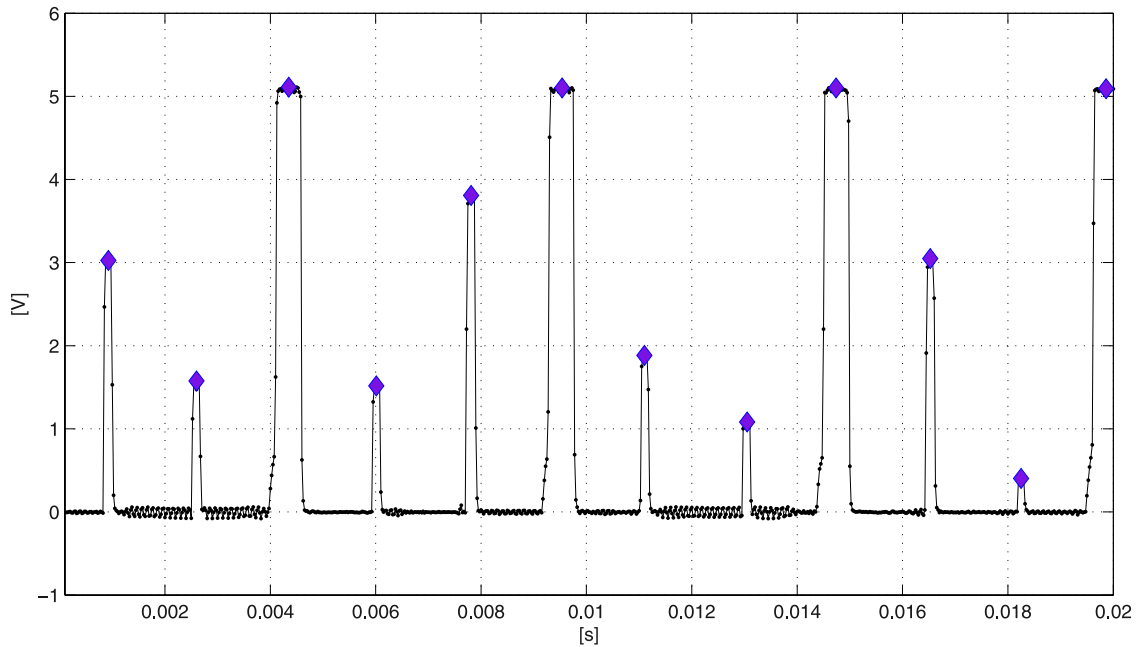
Figure 1. Sample of time signal acquired during calibration. Diamonds indicate the voltage averaged over each single peak.

behind the use of two synchronized SPC lies in the necessity to obtain spatial information at different times (e.g., a mass flux vertical profile) in a process which is not (strictly) in steady conditions. Indeed, snow drift is achieved in the wind tunnel by blowing air on a intact fresh snow surface, with no feeding on the upstream section. Therefore, from a morphodynamical point of view, the conditions are not in equilibrium since there is no mass flux input to balance the erosion process. Moreover the snow cover in the test section does not extend to the whole wind tunnel implying that there is a roughness change upstream (though minimized by the choice of a carpet with similar roughness length scale of the snow) and also a change between a nonerodible and an erodible surface. We indeed observed that, at a fixed wall normal position z_i, measurements of snow drift exhibit fluctuations on timescales much longer than those typical of the saltation process. These large timescale variations are of the order of the measuring time (at each point z_i) that we must choose to obtain a mass flux profile (see the results section). In the work of *Clifton et al.* [2006] it is suggested that in the wind tunnel snow drift measurements should not extend for more than 30 min. Preliminary observations confirmed a systematic dampening of the mass flux after roughly 30 min, thus posing a significant constraint. Although such indications must depend on the snow cover characteristics, obtaining SPC profiles needs a balance between the spatial resolution of the vertical profile (number of points of the profile) and the temporal duration of each point-wise measurement, ultimately affecting the representativeness of the statistics. Two solutions were employed, i.e., 3 min acquisitions and 6 points in the vertical direction, and 1 min acquisition and 11 points in the vertical direction. We are therefore in the situation in which (1) mass flux vertical profiles can be obtained within the maximum allowed time window of observation (30 min); (2) the measured time series are

inferred to be representative of the saltation process at a certain height; (3) boundary conditions are, however, such that large-scale variations can occur; (4) we must monitor the mass flux in time rather than assume equilibrium conditions. Therefore if we want to perform snow drift experiments in a wind tunnel in realistic conditions (i.e., with fresh snow and no external feeding) and obtain temporal and spatial information, two synchronized SPCs are needed. The first SPC was then positioned at roughly 2 cm above the snow surface and continuously recording for the whole observation period of 30 min. The second SPC was moved, together with the anemometer, in the vertical direction. The latter, in alternative to the pressure rake of pitot tubes used by *Clifton et al.* [2006], provided a similarly well resolved mean velocity profile for each experimental conditions.

2.3. SPC High-Frequency Signal

[6] The SPC working principle is based on focused light emitter and a receiver [see, e.g., *Nemoto and Nishimura*, 2001; *Schmidt*, 1982] and reference therein). Electric pulse signals of snow particles passing through a sampling area ($2 \times 25 \times 0.5$ mm) are sent to an analyzing logger. Pulse signals that correspond to the shadow sizes of snow particles are classified into 32 diameter classes. The sensor output consists of a voltage signal that exhibits a peak (above the noise level) with a height proportional to the particle size. Particle counting, particle diameter distribution and mass flux are calculated over a 1 s averaging time and implemented in the SPC hardware and software. However as we will describe in the following, the signal from the SPC sensor can be directly sampled such to obtain the whole time history of all the particles crossing the sensor. For each SPC, two outputs were recorded, namely (1) the typical low-frequency 1 Hz signal (hereinafter referred to as LF signal) of the mass flux and particle size distributions,
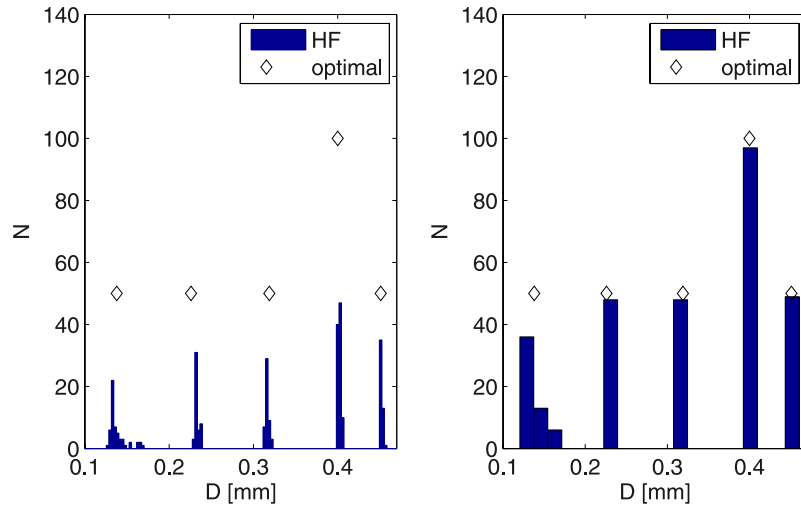
Figure 2. Distribution of the calibration diameters as obtained by the high-frequency (HF) signal during calibration for a (left) fine resolution of 3 μm and a (right) coarse resolution of 20 μm. Diamonds indicate the expected number of realization for each diameter voltage averaged over each single peak.

obtained by the software interface provided by the manufacturers and (2) the high-frequency time signal directly from the sensor, (hereafter referred to as HF signal and sampled at 40 KHz). In order to extract the particle size from each peak of the HF signal we had to calibrate the sensor output using a Niigata calibration device. The SPC sensors have been calibrated at −10C using a set of wires with a known diameter. The calibration test unit was designed such that each wire optimally crosses the sensor observation volume leaving a clear measurable peak in the HF sensor output. A typical realization of the sensor output during calibration is shown in Figure 1.

[7] The frequency at which the peaks are detected depends on the angular velocity of the calibration device. Given a certain observation period, we can therefore exactly calculate, for each diameter, how many peaks we expect to find, and compare it with the results from the processing of the high-frequency SPC signal. The histograms of the estimated diameters in the calibration period should ideally consist of 5 single bin peaks. It is however clear that the binning of the distribution, i.e., the resolution we employ to divide our realizations into diameter classes plays a significant role. In Figure 2 we show the calibration results employing a fine resolution (the estimated sizes are dispersed around the wire size) and a coarser resolution (the estimated sizes collapse on the wire size). The diamond symbols indicate the number of peaks expected through an optimal calibration.

[8] We can use the observed differences to provide an assessment of the calibration procedure, namely we can calculate, for each diameter, what is the percentage of correctly estimated diameters as a function of the error that we accept. We then divide the number of correctly estimated diameters by the number of expected diameters, and we plot it as a function of the relative error (defined as the size of the bin divided by the correspondent diameter). In Figure 3
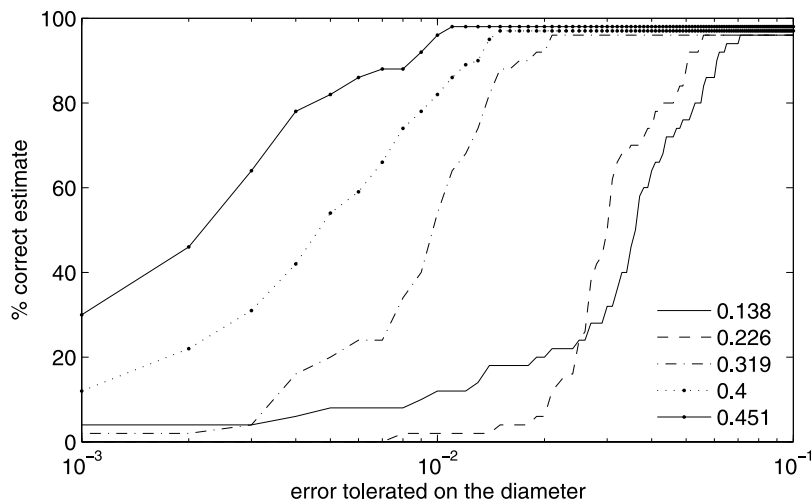

Figure 3. Percentage of the successful estimate as a function of the relative acceptable error for the five calibration wire diameters (listed in the legend in millimeters).
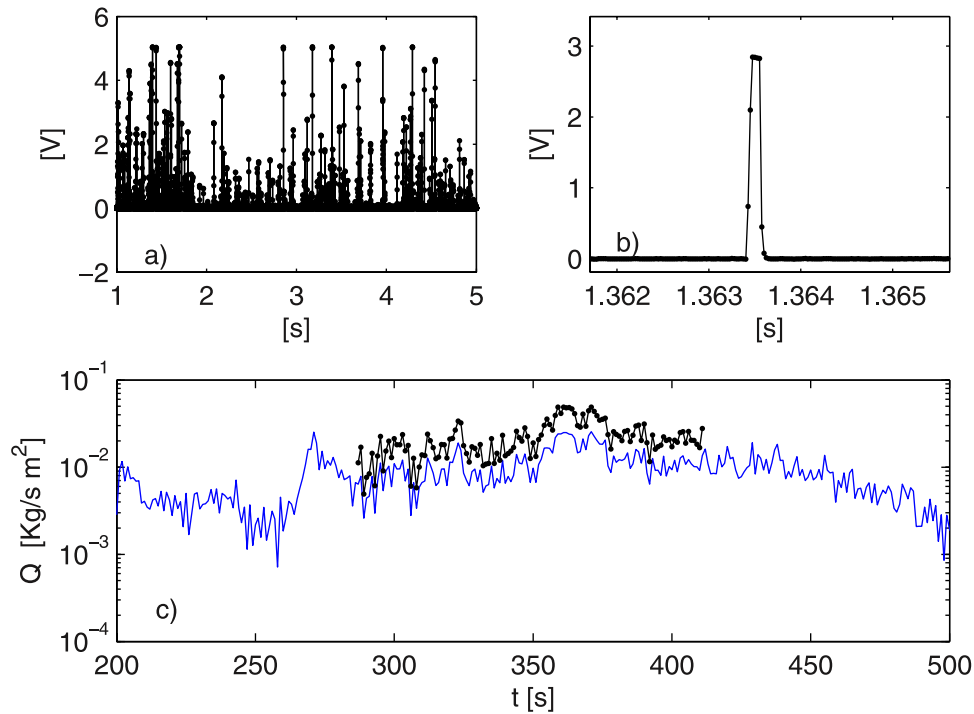
Figure 4. (a) Sample of the HF signal over a 5 s period; note (b) the resolution of each peak. (c) The comparison between the mass flux estimated from the low-frequency (LF) and HF (dots) signals is shown.

we note for instance that small diameter wires are more difficult to estimate, but that, accepting a 7% error on the diameter, we can capture properly more than 97% of them. With a 2% error we can confidently identify wires larger than 0.3 mm, but we have more difficulties with smaller ones. The same analysis on the absolute error shows that the calibration procedure has an accuracy of at least $10\mu m$ (corresponding to more than 95% of success for the smallest wire).

[9] Preliminary observations at varying sampling frequency suggested that at 40 KHz the HF signal was fully resolved and the peaks clearly distinguishable. A peak detection algorithm was developed and tested on the calibration signal. Each peak was detected, recognized as a single realization and unambiguously related to the correspondent wire diameter. The second stage of the testing and calibration procedure consisted in comparing the mass flux and the particle distribution output provided by the SPC software with those extracted by the HF signal during a real snow drift experiment. Indeed the SPC HF signal provides a time history signal (see Figures 4a and 4b) where each snow particle passing through the sensor is detected, its diameter estimated and its contribution to the total mass flux is added. The mass flux is then defined as the sum of the masses of all the particles detected by the sensor in 1 s, divided by the sensor observation area, and it has the dimensions of $Kgs^{-1}m^{-2}$. The comparison between the LF and the HF mass flux integrated over a 1 s interval is shown in Figure 4c). We can see that the result of the processing of the HF signal overestimates the mass flux obtained by the SPC. The ratio between the mean HF mass flux and the mean SPC mass flux is about 1.9. The mean

offset is due to the different way in which the mass flux is computed: from the HF signal, each particle directly contributes to the mass flux, while the SPC uses the average particle diameter for each diameter class. The two estimates become closer for increasing number of diameter classes. The two signals are however very well correlated ($r^2 = 0.98$), implying that the fluctuations of the mass flux are well captured by the HF signal.

3. Results

[10] We now presents results from two wind tunnel experiments. The meteorological conditions at the time of the experiments are summarized in Table 1 together with the flow characteristics. The shear velocity u_* and the roughness scale z_0 are estimated using a standard fitting procedure of the velocity profile in the logarithmic layer obtained by the anemometer. Both parameters were in the range of values reported by *Clifton et al.* [2006, 2007] for fresh snow.

3.1. Mass Flux Profiles and Particle Size Distribution in Height

[11] The experimental setup consisted in two SPCs, at the same stream-wise location. Two SPCs are needed in order to compensate for the large timescale variation observed in the mass flux by a fixed SPC, while the other is moving along the vertical direction. We note indeed that the mass flux at $z_1 = 1.2$ cm is characterized by fluctuations with timescales of the order of $10^1 \sim 10^2$ s, corresponding to the measuring time of the mass flux at each vertical location (see Figure 5). The existence of such large scales is possibly related to large-scale sediment waves slowly evolving in time or to

Table 1. Flow and Environmental Characteristics During the Experiments[a]

Experiment (N Points)	Ambient		Snow ρ_s (kgm^{-3})	Flow Property	
	T (°C)	RH (%)		u_* (ms^{-1})	z_0 (m)
1 (6)	−2.5	65	62	0.49	2.7×10^{-5}
2 (11)	−0.3	77	<100	0.51	5.0×10^{-5}

[a]Here mean temperature is T, relative humidity is RH, snow density is ρ_s, shear velocity is u_*, and roughness length is z_0.

Figure 6. Images of the snow surface after drift; (a and b) note a large-scale sediment wave (it was observed to move slowly in time) in the proximity of the instrumentation. (c) Note the complex surface pattern at the end of the experiment (wind direction was from top to bottom of the image).

small surface forms developing on the snow surface (see Figure 6). The latter contributions must therefore be filtered out in order to estimate the genuine mean vertical variation of the mass flux. Given the length of the wind tunnel, 12 m, the mean velocity of the flow, 10 ms^{-1}, in the free stream velocity, and a few meter per second in the saltation layer, we can safely assume that the largest flow timescale should not exceed a few seconds, regardless of the occurrence of secondary flows or large-scale turbulent motions. For this particular reason we can relate the mass flux signal of the fixed SPC, close to the wall, with the one of the moving SPC, at various heights, such to filter out the very large timescale oscillations observed in Figure 5, when estimating the vertical mass flux profile. We however acknowledge that the evolution of the saltation layer in the occurrence of, relatively slower, surface processes involving erosion and bed forms deserves further investigation.

[12] The necessary steps for the estimate of the mass flux profile are shown in the four patrs of Figure 7 and are as follows: (1) the two SPC time histories are compared in Figure 7a and the periods in which the moving SPC was kept at a certain height are highlighted; (2) the two estimated mass fluxes are compensated such that at the first point (first period), while the two SPC are at the same position, their mean values are equal; (3) the averaged mass flux
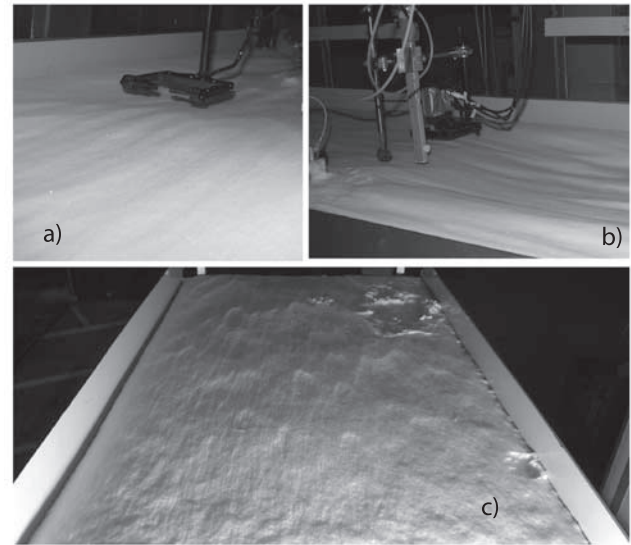
during the following periods are computed and shown in Figure 7b, those represents the large timescale variation of the mass flux; (4) the averaged mass flux from the moving SPC are shown in Figure 7; (5) The latter values are point by point divided by the time averaged mass flux in order to compensate for the large timescale variation (Figure 7d). The latter procedure is also applied for the vertical profile of the particle frequency F.
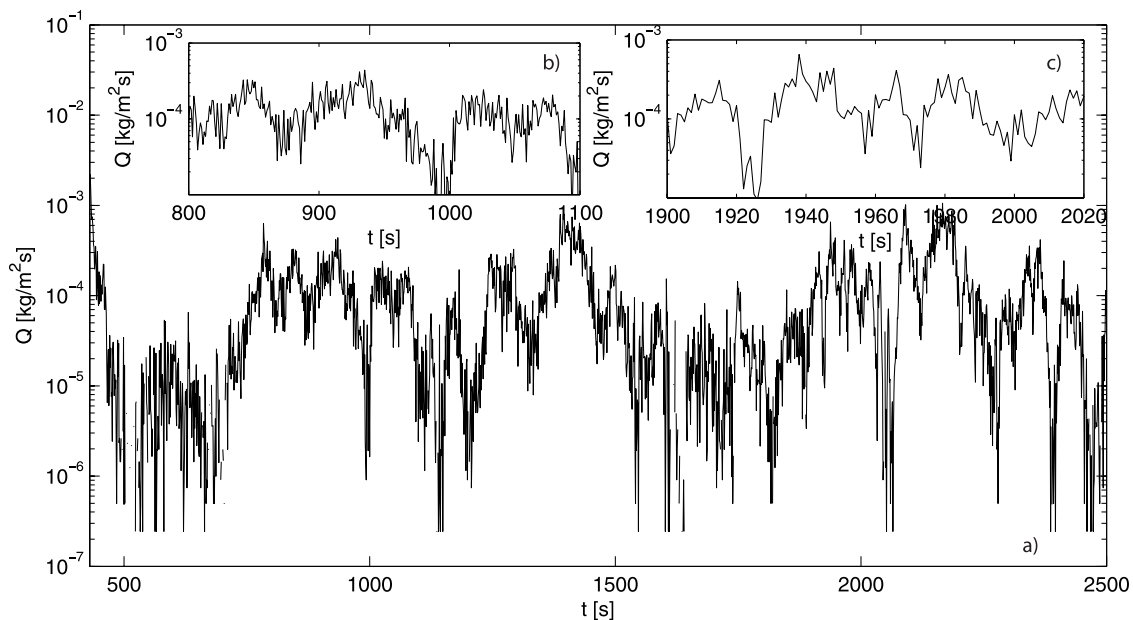

Figure 5. (a) Full time series of the mass flux estimated from the fixed Snow Particle Counters (SPC) $z_1 = 0.012$ m, note some oscillations, with periods of roughly (b) 100 s and (c) 3 s in inlets.
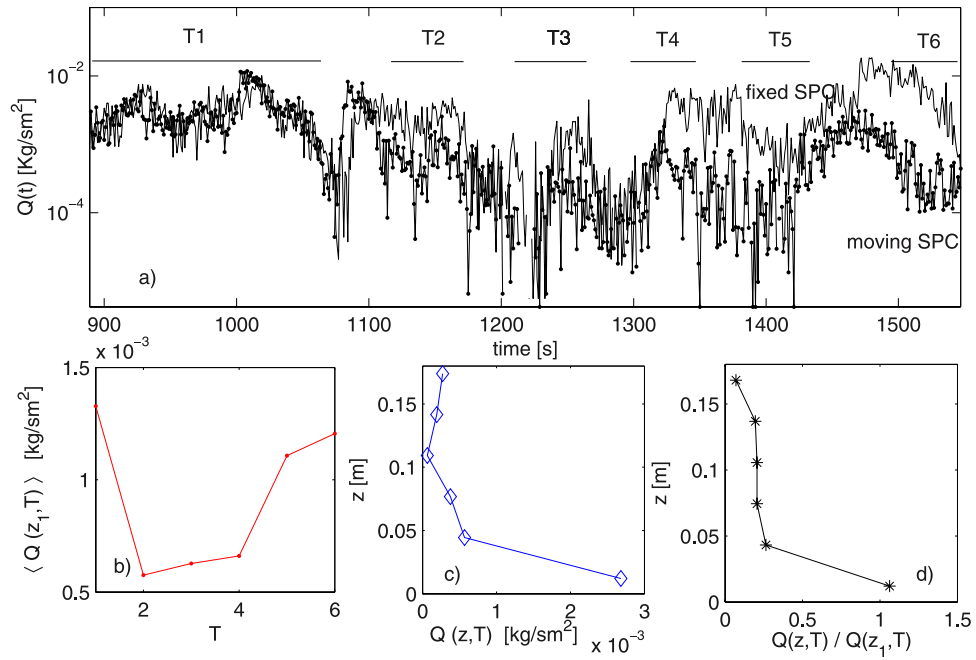
Figure 7. (a) Time series of the mass flux estimated from the moving and the fixed SPC; (b) averaged mass flux of the fixed SPC in the time interval $T(i = 1:6)$ indicated in Figure 7a; (c) raw mass flux profile computed from the moving SPC; and (d) compensated mass flux profile, normalized point by point by the local time averaged mass flux estimated by the fixed SPC at $z_1 = 0.012$ m.
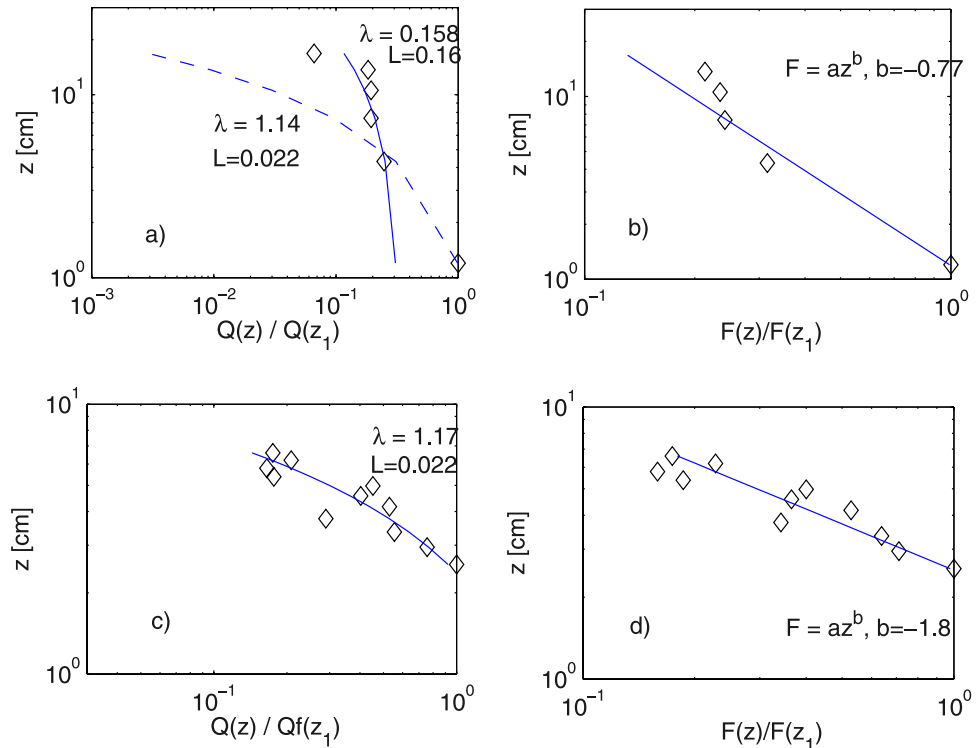

Figure 8. (a and c) Dimensionless compensated mass flux profile and (b and d) particle frequency profiles. Data are from experiment 1 (Figures 8a and 8b) and experiment 2 (Figures 8c and 8d).
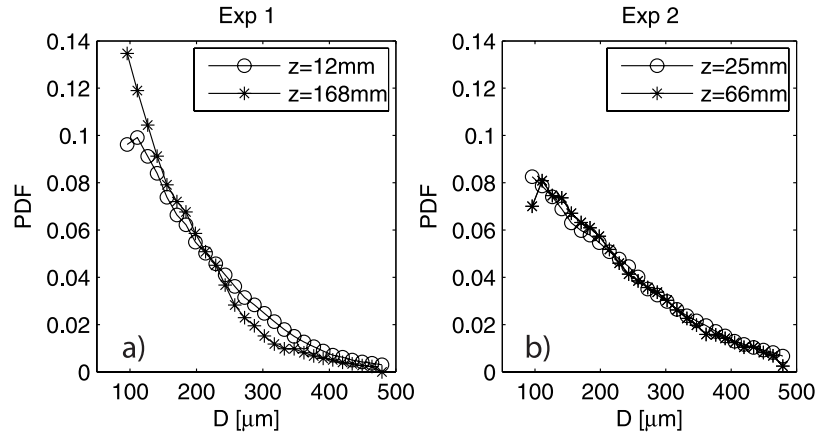
Figure 9. Particle size distribution at different heights for experiment (a) 1 and (b) experiment 2.

[13] *Bagnold* [1941], *Nalpanis et al.* [1993], and *Nishimura and Hunt* [2000] show that the mass of saltating material decreases logarithmically with height. The mass flux profiles they observed, follow the form:

$$q(z) = a_m(u_* - u_{*t})^3 \frac{\lambda g}{u_*^2} e^{\lambda g z / u_*}, \qquad (1)$$

where u_{*t} is the threshold shear velocity, g is the acceleration due to gravity (9.81 m s^{-2}), a_m a constant and λ is a parameter which defines the length scale of the saltation system L, relative to the height a particle reaches when ejected from the surface at vertical velocity u_*, such that $L = \frac{u_*^2}{\lambda g}$. There are then two ways to estimate λ. The first is through mass flux measurements at the same height with varying free stream velocity, hence different u_*, the second is through the shape of the mass flux profile. The latter is preferred since it allows for the estimate of λ independently of the assumed or estimated values of a_m and u_{*t}. The estimate of the threshold velocity, in particular, can be obtained through model-based regression analysis on mass flux measurements at varying u_* [see *Stout and Zobeck*, 1996; *Clifton et al.*, 2006] and should not be chosen a priori because of its strong variability with the snow and meteorological parameters. We can thus use the dimensionless mass flux profile to estimate only the value of λ as it is done by *Nishimura and Hunt* [2000]. The results, shown in Figure 8, are however not straightforward. It should be noted that snow drift can occur in regime of pure saltation, pure suspension or in a mixed saltation-suspension. In the latter case, close to the wall, the mechanism of splash, particle collisions and ejection are dominant, while moving farther from the wall, saltating particles are entrained into suspension, tend to follow long and complex trajectories, and contribute to significant mass flux in the outer layer. For increasing contribution by suspension to the total snow drift, the saltation layer blurs into the suspended material and L becomes more difficult to detect. In the first experiment the measurements extended up to roughly 18 cm, so well above the estimated saltation layer. Despite of that, a nonnegligible mass flux was measured, implying that suspended snow transport was occurring. Choosing different set of points in the fitting procedure toward the estimate

of λ we obtain very different values, from $\lambda = 0.18$ to $\lambda = 1.1$. In particular, including all points, $\lambda = 0.72 \pm 0.13$, $r^2 = 0.85$. However, excluding the first point, as shown in Figure 9a (dotted line), the estimate is significantly altered, leading to $\lambda = 0.15 \pm 0.04$, $r^2 = 0.65$. We thus propose to interpret these values in view of a mixed saltation-suspension regime. The fewer point, we consider, and thus the more we stay close to the wall, the more λ approaches unity (λ increases from 0.7 ($z < 16$cm) to 1.15($z < 8$cm)). A larger value of λ result indeed in a smaller value for L. This means that, if we assume that the only relevant contribution to the mass flux is due to a saltation process, as prescribed in equation (1), the saltation layer must extend to the top of our measurement range and consequently λ approach low values. If we assume instead that saltation is confined to the first 5 cm, then λ approaches unity. We are then in the situation in which results and working assumptions are inherently related. On the one hand by observing the frequency profile in Figure 8b), it is evident that two slopes can be identified and thus some change in the transport mechanism can be inferred. On the other hand only a limited number of points is available close to the surface, so, even assuming a specific height at which suspension is the dominant process, the estimate of λ would not be robust. In the second experiment we have a larger number of points in the proximity of the surface and the frequency profile is well reproduced by a single slope. Furthermore the latter slope is steeper as compared to the previous experiment, as it is expected if we assume negligible transport of snow in suspension. The estimated value of $\lambda = 1.1$ is consistent with the previous estimate but statistically more robust. The fit is indeed carried on using all 11 points, $r^2 = 0.83$ and the r.m.s. error is 0.11 leading to a range of expected value from 1.05 to 1.28. Varying the number of points in the fit from 5 to 11, and including the r.m.s. error, we find that the minimum and maximum values are from 0.95 to 1.3. Averaging among those, we obtain $\lambda = 1.12 + \pm 0.17$. This is the estimate that we consider more robust, also because of the fact that all points are reasonably believed to be inside the saltation cloud ($z < 7$ cm). It is noteworthy that the assumptions of dominant saltation in the second experiment and mixed saltation and suspension in the first experiment (within the investigated vertical range) is supported by the PDF of the grain size distribution (Figure 9). While in the
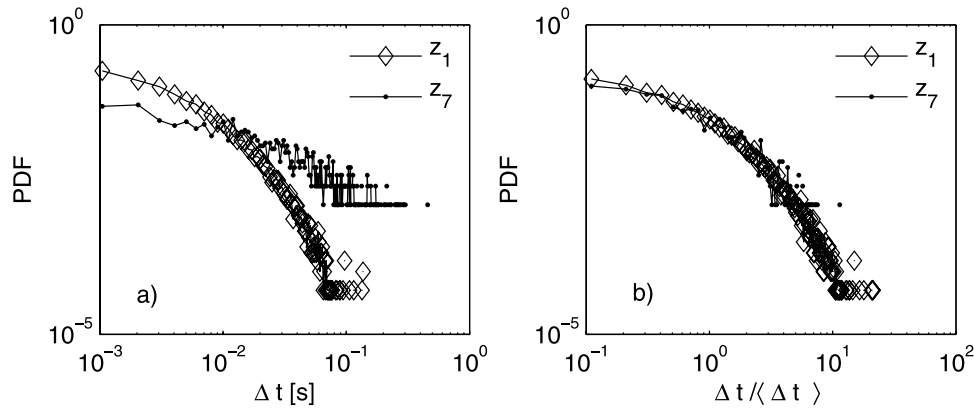
Figure 10. Probability density function of the interparticle time distance Δt (experiment 2). Comparison between the distribution at the surface (z_1) with the one at the upper limit of the saltation layer (z_7) in (a) dimensional and (b) dimensionless units. Note that $\langle \Delta t \rangle_{z1} = 0.0065$ s, $\langle \Delta t \rangle_{z7} = 0.04$ s, at $z_1 = 25$ mm, and $z_7 = 66$ mm, respectively.

former case a significant difference is appreciated by comparing the particle size distribution of the first and last points, in the second experiment the two distributions are almost overlapping, implying that the mass flux height distribution is dominated by the frequency of the saltating particles rather than by their size distribution in height because of suspended load. We must note our estimate of λ is not in agreement with the value of $\lambda = 0.45$ reported by *Nishimura and Hunt* [2000] for round and compacted snow, but it is closer to the one reported by *Pomeroy and Gray* [1990] ($h = 1.6 * u_*^2/2g$, implying $\lambda = 0.8$). There are however several significant differences in these two experiments and a conclusive statement on the optimal estimate of λ cannot be made here. First of all the present experiment is performed with fresh snow and with a real snow cover of more than 10 cm. The experiment is performed immediately after snow fall, such that only a few minutes occurred between the measurements of the first point and the removal of the snow trays from outside into the wind tunnel test section. The second difference is that the saltation layer developing in our wind tunnel cannot be strictly regarded as in equilibrium since no upstream feeding of snow can be provided. So with respect to a natural snow saltation layer, we provide realistic snow particles and a realistic snow surface [see *Loewe et al.*, 2007], while *Nishimura and Hunt* [2000] were able to provide a realistic equilibrium condition. The fact that λ exhibits significant differences implies that the whole saltation process is influenced by the fetch, the roughness and the geometry of the snow particles, including the effect of a dispersed size distribution of snow particles. This is also acknowledged by *Nishimura and Hunt* [2000] when discussing the different values of λ for the different particles employed (snow, ice, sand, mustard seed and wallnut shells). In the next sections we present some results from the high-frequency measurements, aiming to shed some light on the short-timescale behavior of the saltation process.

3.2. Single Point Statistics of Saltating Particles

[14] The SPC high-frequency (HF) signal can be used to size each single particle crossing the sensor observation volume. We now concentrate on the saltation timescale, on the temporal resolution of the mass flux and on the statistical behavior of particles of different sizes.

3.2.1. On the Saltation Timescale

[15] The shortest timescale we can identify is the time interval between two consecutive particles, here and after simply referred to as Δt. The PDF of the distribution of Δt is shown in Figure 10. The range of values is surprisingly large, ranging from 10^{-4} to 10^{-1} s It is however relevant to note that, once normalized with the mean inter particle time $\langle \Delta t \rangle$, the PDFs of Δt close to the snow surface (z_1) and at the upper limit of the saltation layer (z_7) collapse, suggesting that $\langle \Delta t \rangle$ is one of the relevant timescales of the saltating process.

[16] Since the saltation layer is formed by particles of different diameters, we can compute Δt for classes of particles with a similar size (see Figure 11). We note that large particles are on average separated by larger time interval when compared to smaller size particles. Despite of that, large particles are still expected to contribute dominantly to the mass flux. Indeed a factor 5 in the particle diameter, implies a factor of 5^3, i.e., 2 order of magnitudes, in the mass flux, while the difference in the $\langle \Delta t \rangle$ is only 1 order of magnitude when comparing $D = 0.1$ mm, with $D = 0.5$ mm particles. Therefore the rare occurrence of large particles only partially compensates for their larger size. An accurate model of the threshold of motion of the large particles, as well as their entrainment into suspension, would then strongly contribute to the prediction of the mass flux.

[17] The contribution of the large particles to the mass flux plays also a role in the normalized profile of the mean interparticle time interval $\langle \Delta t \rangle$. The profile is derived with the same procedure employed with the mass flux, i.e., by taking into account the large timescale variations captured by the fixed SPC. The characteristic timescale and length scale in the saltation process, chosen for normalization, are u_*/g and $L = u_*^2/(\lambda g)$ respectively, consistently with the key role played by the shear velocity and the acceleration of gravity on the trajectories of saltating particles and on the parameterization of sediment and eolian transport [see, e.g., *Anderson et al.*, 1991; *Nalpanis et al.*, 1993; *Butterfield*, 1999].
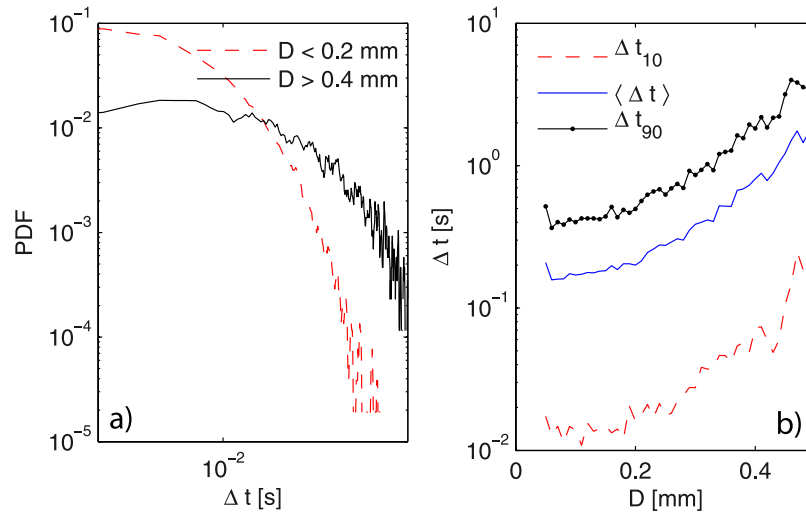
Figure 11. (a) Probability density function of the interparticle time distance Δt, at the location $z_1 = 25$ mm, for coarse and fine particles. (b) The mean Δt and the values corresponding to the 10 and 90 percentile of the distribution is plotted as a function of the diameter D.

[18] In Figure 12a the profile is plotted in dimensional units. We note that for $z = 5 \sim 6$ cm there is a slight change in the shape of the $\langle \Delta t \rangle$ profile. We can speculate that $h = 6$ cm is approximately the top of the saltation layer. The latter scale is not however statistically representative of the height of the saltating particles, since it rather defines their upper limit. Assuming $\lambda = 1$, as previously estimated from the mass flux profile, we obtain $L = 2.5$ cm which is approximately half of the inferred height of the saltation layer. It is however legitimate to ask why $\langle \Delta t \rangle/(u_*/g) < 1$ in the core of the saltation layer, i.e., for $z/L \sim 1$ (see Figure 12b). The answer lies in the heterogeneity of the size distribution. Indeed $\langle \Delta t \rangle$ does not take into account the size of the particles, but only their occurrence in time. As a result of this, $\langle \Delta t \rangle$ is representative of the most common particle (in size) rather than of the larger ones, that mostly contribute to the mass flux. From another point of view, we also infer that the very small particles, most probably in suspension and negligible for the mass flux parametrization, result in an underestimation of $\langle \Delta t \rangle$. We thus suggest that values of $\langle \Delta t \rangle/(u_*/g) \simeq 1$ occur at $z/L \simeq 1$ in case of monodispersed

distributions of particle sizes, i.e., of mass flux solely determined by the particle frequency. We also suggest that in the case of dispersed distribution of particle sizes, λ must be estimated through the mass flux profile rather than the particle frequency or the equivalent $\langle \Delta t \rangle$ profiles.

3.2.2. On the Optimal Temporal Resolution of the Mass Flux

[19] Now that the mean interparticle time interval $\langle \Delta t \rangle$ is regarded as a relevant timescale of the saltation process, we can focus our attention on the definition of mass flux as a continuous time signal. The question is whether it is possible to use $\langle \Delta t \rangle$ to derive the minimum timescale over which a mass flux can be defined. As we observed in Figure 10 the time interval between particle varies considerably spanning 3 orders of magnitude in the range between 10^{-3}s to 10^0 s, depending on the vertical location. A possible way to define the best resolved mass flux is to check for "holes" or missing points in the mass flux computation as a function of the time resolution δt. In each δt the mass flux is defined as the sum of the contribution of all the particles crossing the sensor in that time interval. In Figure 13 we observe that
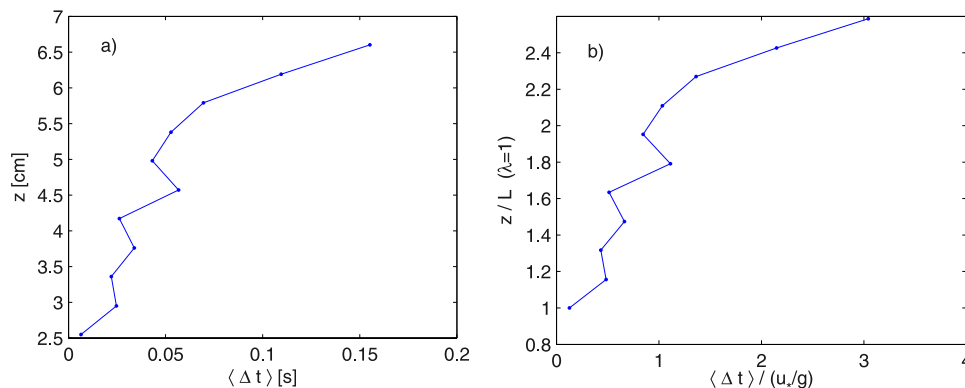

Figure 12. Vertical profile of the mean interparticle time interval Δt (a) in dimensional units, (b) normalized with the timescale u_*/g. (L is computed assuming $\lambda = 1.0$.)
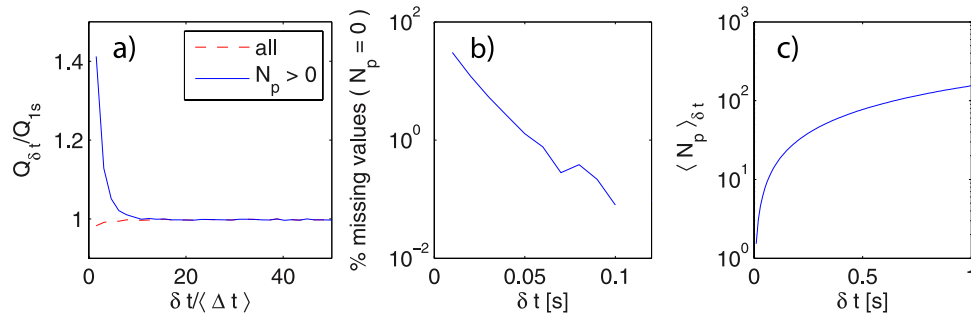
Figure 13. Mass flux as a function of the time resolution δt. (a) The mass flux for varying δt is compared to the one averaged over 1 s, when computed over all the values or only the nonzero ones (always particles detected in that time interval). Note that the time resolution is normalized with the mean interparticle time interval $\langle \Delta t \rangle$. (b and c) The percentage of missing values (no particles detected) and the number of detected particles, is computed as function of the time resolution δt, respectively.

(1) with $\delta t = 0.1$ s, the mass flux is consistent with the estimated mass flux averaged over 1 s; (2) it has a negligible percentage of missing points; (3) in terms of mean interparticle time, it corresponds to roughly $10 \sim 15 \langle \Delta t \rangle$. The latter timescale (in this specific context) is regarded to as the optimal temporal resolution, in the sense that it allows for the most detailed description of the mass flux.

3.2.3. On the Assumption of Monodispersed Particle Size in a Realistic Saltation Layer

[20] In this section we focus on the short-timescale behavior of saltating particles of different size. The heterogeneity of the particle size distribution is indeed a genuine feature of a realistic snow saltation layer and it thus deserves particular attention. While in suspension regime the heterogeneity of the distribution of the particle sizes is important, as discussed by *Xiao et al.* [2000] and *Dery and Taylor* [1996], in the context of mass flux modeling in saltation regime, it is common practise to assume a single representative particle diameter instead of a size distribution. Such assumptions must be inherently related to the desired time resolution of the mass flux signal, since the peculiar

behavior of relatively small and large particles must be averaged out, (e.g., variations of the mass flux on a minute scale do not depend on the different statistical behavior of fine and coarse saltating particles). Given the diameter and the occurrence of each particle, we can define a coarse and a fine fraction of the mass flux and compare the two signals. It is natural to expect that for large timescales the coarse and the fine fractions behave similarly. However the two mass flux signal are supposed to get decorrelated while increasing the time resolution (thus decreasing the timescale on which the mass flux is computed). The question on the decorrelation of the coarse and the fine snow particle fractions may be related to the timescale during which different particles, belonging to the same group, tend to cluster in the time series. On the one hand, the underlying physics of a saltation layer indeed suggests that collisional mechanisms, splash and ejections should trigger the detachment of group of particles rather than just one particle at the time. On the other hand, when the saltation layer is in equilibrium, it is natural to expect that the signature of each single splash is averaged out and possible clusters of particles get mixed
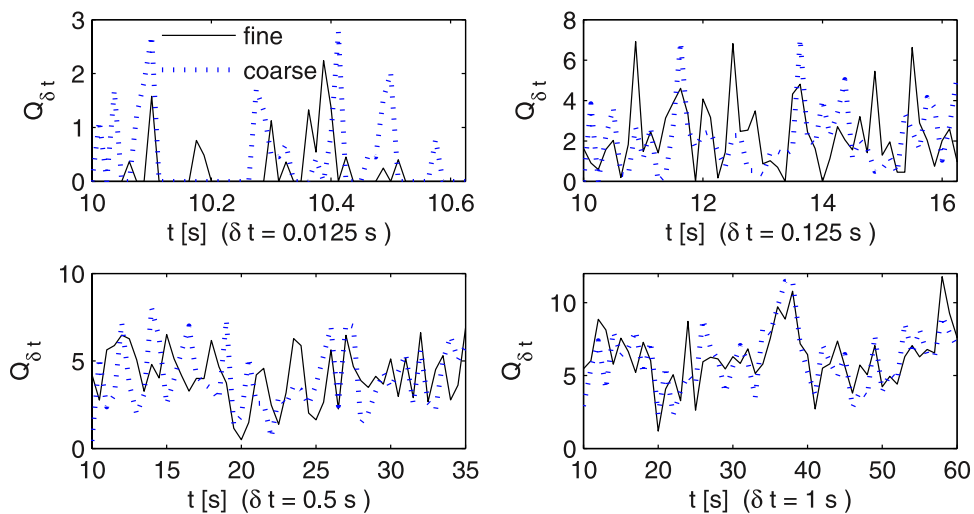

Figure 14. Time history of the dimensionless mass fluxes of the coarse and fine fraction, respectively, for different moving average windows Δt. Note that of the mass flux of each fraction is normalized by its standard deviation.
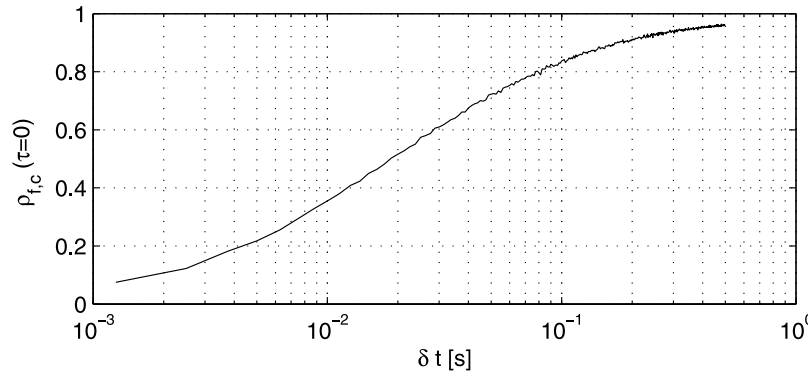
Figure 15. Peak of the cross correlation coefficient between the coarse and the fine fraction of the mass flux as a function of the averaging time δt.

and hardly detectable. In Figure 14 we show the time signal of the contributions of the fine and coarse fractions of the snow particles, normalized to the total mass flux, and derived by averaging over four different time periods, i.e., time resolution, δt. It is clear that the two time histories shown in Figure 14 tend to overlap for increasing averaging time, implying that the observed mass flux variation are due to the occurrence of large flux of particles comprehending both large and small ones. This trend indicates that, at a certain timescale, we cannot distinguish anymore between the fine and large diameter contributions. The total mass flux is thus governed by large-scale fluctuations that capture fine and coarse particles indistinctly.

[21] In order to quantify the trend outlined in Figure 14, we compute the cross correlation between the fine and the coarse mass flux functions. The peak of the cross correlation, located at the zero time lag, increases with the averaging time, since the two fractions are more and more in phase. We can quantify this relationship in Figure 15 where $\rho_{f,c}(\tau = 0)$ is plotted as a function of δt. We can distinguish three regions, (1) $\delta t < 0.01$ s $\simeq \langle \Delta t \rangle$, where the two signals are substantially decorrelated because of the rare occurrence of a particle; (2) $\delta t > 0.1$ s $\simeq 10 \langle \Delta t \rangle$, where the peak tends to approach the full correlation $\rho_{f,c}(0) = 1$; (3) a buffer region which might indicate the range of timescales covered by groups of particles formed by coarse and fine snow crystals. This range of timescales, especially in the upstream section of a saltation layer, might be related to a collisional timescale, i.e., a time interval between the splash of one particle and the ejection of new particles. In that case, however, the peak of the cross correlation might be shifted toward some lag $\tau \neq 0$, which was not observed in our case. In equilibrium condition, instead, such results suggest that for a mass flux averaged over $\simeq 10 \langle \Delta t \rangle$ the simplifying assumptions of single size distribution can provide substantially correct results since the fine and the coarse fractions behave similarly. As a definition of coarse and fine fraction we employed the following: (1) $D < D_{30} \sim 0.12$ mm belong to fine and (2) $D > D_{70} \sim 0.25$ mm belong to coarse. Despite the above definition being arbitrary, we did not notice significant qualitative changes in the observed trend for the different boundaries. We must however note that, because of inertia, small particles will probably have a smaller lag (higher-frequency response) than large particles and therefore show less decorrelation to flow but increas-

ingly decorrelation to large particles. It is noteworthy that this analysis is able to provide quantitative information on the representativeness of a single diameter input (usually the mean) in the mass flux predictions provided by models, depending on the resolved timescale and ultimately on the physical mechanism that the model is able to reproduce.

4. Conclusions

[22] In this contribution we presented experimental results on the saltation of fresh snow particles obtained in a wind tunnel with a real fresh snow surface, controlled flow and monitored environmental conditions. On the experimental side we propose a novel technique to capture and analyze the high-frequency behavior of saltating particles on the basis of the calibration and direct acquisition of the SPC sensor output signal; we further suggest a procedure to compute the vertical profiles of the mass flux by using two SPCs in order to compensate for the significant large timescale variation of the mass flux observed by the SPC kept at a fixed position close to the snow surface. We indeed observe that the development of the saltation layer in the wind tunnel with erodible fresh snow surface and in the absence of external feeding, exhibit a surprising range of timescales ranging from $O(10^{-2})$ to $O(10^{2})$ s, respectively associated with the mean time interval between saltating particles $\langle \Delta t \rangle$ and with the morphodynamic evolution of the snow surface. While the former scale $\langle \Delta t \rangle$ is regarded as the dominant scale of the saltation process, the latter scale is associated to the propagation of a sediment wave and must therefore be filtered out. The novelty of the present paper is twofold. It provides measurements of the mass flux profile in a saltation layer developing over an intact fresh snow cover in a controlled flow facility with realistic alpine environmental conditions [see *Clifton et al.*, 2006]. It further provides an attempt to describe some aspects of the saltation regime in terms of mean interparticle time interval $\langle \Delta t \rangle$. Indeed, (1) when scaled by $u*/g$, the profile of $\langle \Delta t \rangle$ provide an estimate of the vertical extent of the saltation layer ($\langle \Delta t \rangle / (u*/g) \simeq 1$); (2) the optimal time resolution for the computation of the mass flux as a continuous signal is roughly given by $10 \langle \Delta t \rangle$; (3) The latter also represents the averaging timescale by which the coarse and the fine contributions to the mass flux are well correlated. It is thus representative of the whole saltating process, since the effects associated

with the heterogeneity of the size distribution are not crucial for that resolution. Indeed, a monosized distribution with a properly chosen representative diameter, can be assumed and the large-scale fluctuation of the mass flux can be still captured, as done by *Doorschot and Lehning* [2002]. From the analysis of the mass flux profile we find that $\lambda \simeq 1$ fits well the measurements close to the surface where saltation is the dominant process. We discuss this results emphasizing the role played by the geometry of fresh snow particles, by its heterogenous size distribution and by the roughness properties of the fresh snow. Our results provide a lower estimate of the characteristic height of the saltation layer as compared to previous results where compacted snow particles where used [*Nishimura and Hunt*, 2000]. We must however acknowledge that such difference might also be related to the developing saltation layer as compared to the equilibrium conditions guaranteed by *Nishimura and Hunt* [2000] by feeding snow particles at the wind tunnel inlet. We therefore stress that measurements of mass profile in regime of pure saltation are still required in order to distinguish the effect of the fetch from the one of the geometrical and mechanical properties of both the snow particles and the snow surface (both complex in shape and fragile). Such experiments must be carried on in the field with particular care on the estimate of u_* and on the occurrence of suspended load or in a wind tunnel with real, intact snow cover, real snow particles and measurements at varying fetch. In the framework of sediment transport, the analysis presented here can be applied also to aeolian transport [see, e.g., *Rasmussen and Sorensen*, 2008, and reference therein] and possibly sand transport in rivers, hopefully leading toward a common interpretation of saltation timescales. We however stress that this work is focused solely on the saltation regime, whereas most intense mass transport events in multiphase geophysical flows occurs in suspension regime [see, e.g., *Bintania*, 2002]. More work is needed to study the mutual influence of saltation and suspension as well as the parameterization and the key scaling of a layer in a transitional saltation to suspension regime. Further work is also needed to relate the spatial evolution of the saltation layer to the observed large timescale variation of the mass flux, in view of the role played by sediment waves, surface forms and erosion.

References

Anderson, R. S., M. Sorensen, and B. B. Willetts (1991), A review of recent progress in our understanding of aeolian sediment transport, *Acta Mech. Suppl.*, 1, 1–19.

Anschutz, H., O. Eisen, W. Rack, and M. Scheinert (2006), Periodic surface features in coastal East Antarctica, *Geophys. Res. Lett.*, 33, L22501, doi:10.1029/2006GL027871

Araoka, K., and N. Maeno (1981), Dynamical behaviour of snow particles in the saltation layer, *Proceedings of the Third Symposium on Polar Meteorology and Glaciology*, edited by K. Kusunoki, pp. 253–263, Nat. Inst. of Polar Res., Tokyo.

Bagnold, R. A. (1941), *The Physics of Blown Sand and Desert Dunes*, Chapman and Hall, New York.

Balakumar, B. J., and R. J. Adrian (2007), Large- and very-large-scale motions in channel and boundary-layer flows, *Phil. Trans. R. Soc. London Ser. A*, 365(1852), 665–681.

Bintania, R. (2002), A new power law relation for the vertical distribution of suspended matter, *Boundary Layer Meteorol.*, 104, 305–317.

Butterfield, G. R. (1999), Nar bed mass flux profiles in aeolian sand transport: High-resolution measurements in a wind tunnel, *Earth Surf. Processes Landforms*, 24, 393–412.

Clifton, A., and M. Lehning (2008), Simulations of wind tunnel snow drift using a semi-stochastic model, *Earth Surf. Processes Landforms*, doi:10.1002/esp.1673, in press.

Clifton, A., J. D. Ruedi, and M. Lehning (2006), Snow saltation threshold measurements in a drifting snow wind tunnel, *J. Glaciol.*, 52(179), 585–596.

Clifton, A., C. Manes, J. D. Ruedi, M. Guala, and M. Lehning (2007), On shear driven ventilation of snow, *Boundary Layer Meteorol.*, 126, 249–261, doi:10.1007/s10546-007-9235-0..

Dery, S. J., and P. A. Taylor (1996), Some aspects of the interaction of blowing snow with the atmospheric boundary layer, *Hydrol. Processes*, 10(10), 1345–1358.

Doorschot, J. J. J., and M. Lehning (2002), Equilibrium saltation: Mass fluxes, aerodynamic entrainment, and dependence on grain properties, *Boundary Layer Meteorol.*, 104(1), 111–130.

Doorschot, J. J. J., M. Lehning, and A. Vrouwe (2004), Field measurements of snow-drift threshold and mass fluxes, and related model simulations, *Boundary Layer Meteorol.*, 113(3), 347–368.

Guala, M., S. E. Hommema, and R. J. Adrian (2006), Large-scale and very-large-scale motions in turbulent pipe flow, *J. Fluid Mech.*, 554, 521–542.

Lehning, M., P. B. Bartelt, R. L. Brown, C. Fierz, and P. Satyawali (2002), A physical SNOWPACK model for the Swiss avalanche warning. Part II: Snow microstructure, *Cold Reg. Sci. Technol.*, 35(3), 147–167.

Lehning, M., H. Loewe, M. Ryser, and N. Radershall (2007), Inhomogeneous precipitation distribution and snow transport in steep terrain, *Water Resour. Res.*, 44, W07404, doi:10.1029/2007WR006545.

Li, S. S., and M. Sturm (2002), Patterns of wind-drifted snow on the Alaskan arctic slope, detected with ERS-1 interferometric SAR, *J. Glaciol.*, 48(163), 495–504.

Loewe, H., L. Egli, S. Bartett, M. Guala, and C. Manes (2007), On the evolution of the snow surface during snowfall, *Geophys. Res. Lett.*, 34, L21507, doi:10.1029/2007GL031637.

Maeno, N., K. Nishimura, K. Sugiura, and K. Kosugi (1995), Grain size dependence of eolian saltation lengths during snow drifting, *Geophys. Res. Lett.*, 22(15), 2009–2012.

Massom, R. A., V. I. Lytle, A. P. Worby, I. Allison, and N. Maeno (1998), Winter snow cover variability on East Antarctic sea ice, *J. Geophys. Res.*, 103, 24,837–24,855.

Nalpanis, P., J. C. R. Hunt, and C. F. Barrett (1993), Saltating particles over flat beds, *J. Fluid Mech.*, 251, 661–685.

Nemoto, M., and K. Nishimura (2001), Direct measurement of shear stress during snow saltation, *Boundary Layer Meteorol.*, 100, 149–170.

Nishimura, K., and J. C. R. Hunt (2000), Saltation and incipient suspension above a flat particle bed below a turbulent boundary layer, *J. Fluid Mech.*, 417, 77–102.

Nishimura, K., and M. Nemoto (2005), Blowing snow at Mizuho station, Antarctica, *Phil. Trans. R. Soc. London Ser. A*, 363, 1647–1662.

Pomeroy, J. W., and D. M. Gray (1990), Saltation of snow, *Water Resour. Res.*, 26(7), 1583–1594.

Rasmussen, K. R., and M. Sorensen (2008), Vertical variation of particle speed and flux density in aeolian saltation: Measurement and modeling, *J. Geophys. Res.*, 113, F02S12, doi:10.1029/2007JF000774.

Schmidt, R. A. (1982), Vertical profile of wind speed, snow concentration and humidity in blowing snow, *Boundary Layer Meteorol.*, 23, 223–246.

Stout, J. E., and T. M. Zobeck (1996), The Wolfforth field experiment: A wind erosion study, *Soil Sci.*, 161(9), 616–632.

Sugiura, K., K. Nishimura, and N. Maeno (1998), Measurements of snow mass flux and transport rate at different particle diameters in drifting snow, *Cold Reg. Sci. Technol.*, 27(2), 83–89.

Xiao, J. B., R. Bintanja, and S. J. Dery (2000), An intercomparison among four models of blowing snow, *Boundary Layer Meteorol.*, 97(1), 109–135.

_____

A. Clifton, M. Guala, M. Lehning, and C. Manes, Swiss Federal Institute for Snow and Avalanche Research, Fluelastrasse 11, Davos CH-7260, Switzerland. (guala@slf.ch)